Journal of Power Sources 217 (2012) 351–357

Contents lists available at SciVerse ScienceDirect

Journal of Power Sources

journal homepage: www.elsevier.com/locate/jpowsour

Short communication

Facile approach to synthesize SnO_2 nanoparticles@carbon nanofibers as anode materials for lithium-ion battery

Weiwei Xia [a], Yewu Wang [a,*], Yafei Luo [a], Jiayun Li [b], Yanjun Fang [a], Lin Gu [a], Jiajian Peng [b,*], Jian Sha [a,*]

[a] Department of Physics & State Key Laboratory of Silicon Materials, Zhejiang University, Hangzhou 310027, PR China
[b] Key Laboratory of Organosilicon Chemistry and Material Technology of Ministry of Education, Hangzhou Normal University, Hangzhou 310012, PR China

HIGHLIGHTS

- A simple process to fabricate SnO_2 NPs@carbon nanofibers as anode materials.
- Controlled introduction of carbon to optimize the lithium-ion battery performance.
- This method is easy preparation, low cost, and non-toxic source materials.

ARTICLE INFO

Article history:
Received 20 March 2012
Received in revised form
22 May 2012
Accepted 25 May 2012
Available online 12 June 2012

Keywords:
Tin oxide
Carbon nanofibers
Lithium-ion battery
Anode materials

ABSTRACT

SnO_2 nanoparticles (NPs)@carbon nanofibers as anode materials for lithium-ion battery are synthesized by a novel facile route using the commercial filter paper and tin dichloride dehydrate ($SnCl_2 \cdot 2H_2O$). The weight ratio between carbon nanofibers and SnO_2 NPs, which seriously affects the battery performance, has been demonstrated to be easily tuned by adjusting the sintering temperature. The electrochemical investigations show that the SnO_2 NPs@carbon nanofibers with 9 wt% carbon have the best performance with the highest capacity of 383 mAh g^{-1} after 30 cycles at a current density of 100 mA g^{-1}. The method introduced in this study provides an easy strategy for the controlled introduction of carbon to optimize the performance of lithium-ion battery using SnO_2 NPs@carbon nanofibers as anode materials.

1. Introduction

SnO_2 has been considered as one of the most promising candidates for meeting the increasing requirements of next generation electrode materials for lithium-ion batteries owing to its high theoretical storage capacity of 782 mAh g^{-1} which is more than twice of the currently commercialized graphite anodes (372 mAh g^{-1}) and has lower potential of lithium-ion intercalation compared to that of carbon [1,2]. However, the practical application of SnO_2 is hampered by the rapid decrease in their capacity caused by the quick aggregation of active particles and the huge volume change (over 250%) during the lithiation/delithiation process [3,4]. The huge volume change generates a large internal stress, leading to pulverization of the electrode and electrical detachment of the active particles.

Currently, there are two common strategies which have been pursued in the literature to alleviate this problem. One strategy is to design the various complex SnO_2 nanostructures with large surface-to-volume ratio, such as nanorods [5], nanowires [6], nanoneedles [7], nanosheets [8]and so forth, which have been designed to improve the lithium storage performance of tin dioxide. Although the performance has been improved a lot, it is difficult to synthesize the products in large scale for industrial applications. Another effective approach has been focused on synthesizing composites with other materials to optimize the cyclability of SnO_2. Carbon matrix usually acts as the structural buffer for the large volume change and prevents agglomeration of SnO_2, resulting great performance improvements. Up to now, various tin dioxide-based carbon composite anode materials, such as tin oxide–graphite [9], tin oxide–graphene [10], tin oxide–carbon nanotubes [11], etc., have been prepared, and their electrochemical performances have been investigated. However, the introduction procedure of carbon in composite material was usually complicated and costly [12–15], which limited their practical applications. Herein, we report a simple one-step process to

* Corresponding authors. Tel./fax: +86 571 87953746.
E-mail addresses: yewuwang@zju.edu.cn (Y. Wang), jjpeng@hznu.edu.cn (J. Peng), phyjsha@zju.edu.cn (J. Sha).

0378-7753/$ – see front matter © 2012 Elsevier B.V. All rights reserved.
http://dx.doi.org/10.1016/j.jpowsour.2012.05.072

fabricate large-scale SnO_2 NPs@carbon nanofibers as anode materials for lithium-ion battery. The commercial filter paper and tin dichloride dehydrate are used as the carbon precursor and tin sources, respectively. The key features of this method are easy preparation, low cost, mass production and non-toxic source materials. Moreover, the method provides an easy strategy for the controlled introduction of carbon to optimize the performance of lithium-ion battery using SnO_2 NPs@carbon nanofibers as anode materials.

2. Experimental section

2.1. Synthesis of SnO_2 NPs@carbon nanofibers

In a typical and facile synthesis of the SnO_2 NPs@carbon nanofibers, 0.1 mol of tin dichloride dehydrate ($SnCl_2 \cdot 2H_2O$) was dissolved in 100 mL of ethanol. The solution was then transferred into the conical flask, sealed, and stirred at 70 °C for 4 h. Subsequently, the commercial filter papers (quantitative ashless, Grade No.41, Whatman) were immersed in the solution for 24 h at room temperature, and dried at 80 °C. The treated filter papers were finally sintered at 400–500 °C in muffle furnace under atmosphere.

The weight of a piece of filter paper is 0.7710 g. The weight of the treated filter paper without sintering is increased to 1.2828 g. It can be calculated that the weight ratio of oxides of tin to the empty filter paper in the starting material is 1:1.5.

2.2. Characterizations

Crystallographic information of the as-prepared composites was characterized by X-ray powder diffraction (XRD) using a Rigaku D/max-ga X-ray diffractometer with graphite monochromatized Cu K_α radiation ($\gamma = 1.54178$ Å). The morphology of the as-prepared samples was investigated by field-emission scanning electron microscopy (FESEM, Hitachi S-4800) at an accelerating voltage of 10 kV and the chemical compositions were analyzed by energy dispersive X-ray spectroscopy (EDS). Transmission electron microscopy (TEM) images and the corresponding selected-area electron diffraction (SAED) pattern were captured on a Philips CM 200UT microscope at an accelerating voltage of 160 kV. Thermogravimetric analysis (TGA) was performed on SDT Q600 V8.2 Bulid 100 in air with a heating rate of 10 °C min^{-1}.

2.3. Electrochemical measurements

The working materials were composed of SnO_2 NPs@carbon nanofibers, conductive materials (acetylene black, AB), and binder (polyvinylidene difluoride, PVDF) in a weight ratio of 80:10:10. The prepared working materials were dispersed in N-methyl pyrrolidone (NMP) and then stirred using a magnetic stirrer for about 12 h. Commercial foam nickel was cut into circular shape (12 mm in diameter) and then immersed in the slurry for several minutes. All the immersed foam nickel plates were dried at 120 °C under vacuum overnight. Finally the treated foam nickel plates were pressed on an empty foam nickel plate under a pressure of 10 MPa for 10 s, which acted as the working electrode of the half coin cells. Electrochemical performance was tested by assembling CR2025 half coin cells in a glove box filled with ultra-pure argon, using lithium metal as the counter electrode. A micro-porous polypropylene film (Celgard 2400) was selected as a separator, and a 1 M solution of $LiPF_6$ in ethylene carbonate (EC) and diethyl carbonate (DEC) (1:1 by volume) was used as the electrolyte. The

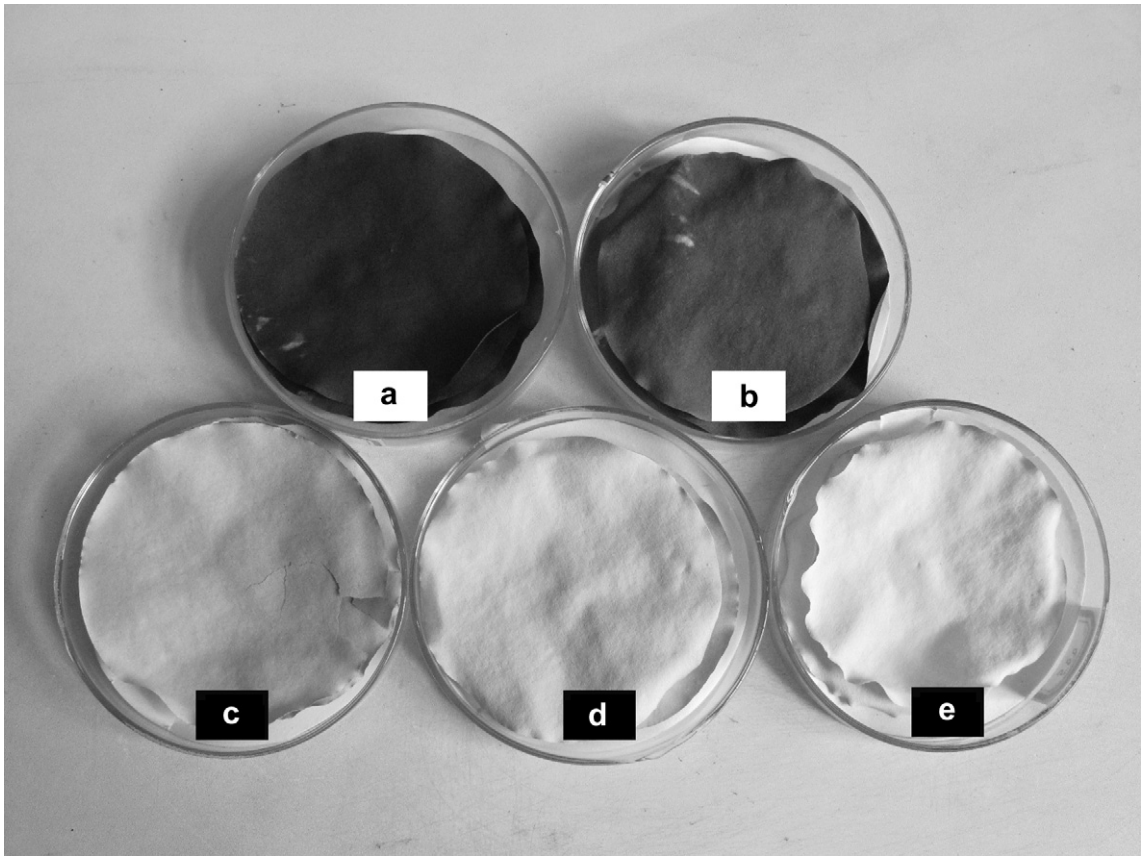

Fig. 1. Photographs of the obtained SnO_2@carbon nanofibers prepared at different calcinations temperatures in air: (a) 400 °C, (b) 425 °C, (c) 450 °C, (d) 475 °C, (e) 500 °C.

galvanostatic charge–discharge was conducted with a Battery Tester (Neware). The cells were cycled at a current density of 50 mA g^{-1} for the first two cycles and 100 mA g^{-1} for the following cycles in the potential range of 0.005–1.5 V at room temperature.

3. Results and discussion

Fig. 1 shows the photographs of the samples sintered at different temperatures. It clearly reveals that the color of the sample becomes more and more white with increasing sintering temperature. EDS spectra taken from the samples prepared at 400 and 500 °C are shown in Fig. 2. The carbon in the sample almost disappears when the sintering temperature increases to 500 °C, which illuminates the color change of the sample with increasing the sintering temperature. The XRD patterns of the prepared samples are shown in Fig. 3. All the characteristic diffraction peaks can be assigned to the tetragonal structure (P42/mnm No. 136, JCPDS 41-1445) of SnO_2 with lattice parameters of a = b = 4.7386 Å and c = 3.1865 Å. No obvious signals from possible impurities such as SnO or Sn residue are observed in the patterns. The absence of carbon peaks can be ascribed to the formation of amorphous carbon nanofibers. In addition, the intensities of the peaks located at 26.4°, 33.87°and 51.92° increase significantly and their full width at half maximum (FWHM) decreases markedly with increasing the sintering temperature. This indicates that crystallization of the SnO_2 NPs becomes better gradually and the crystallite size

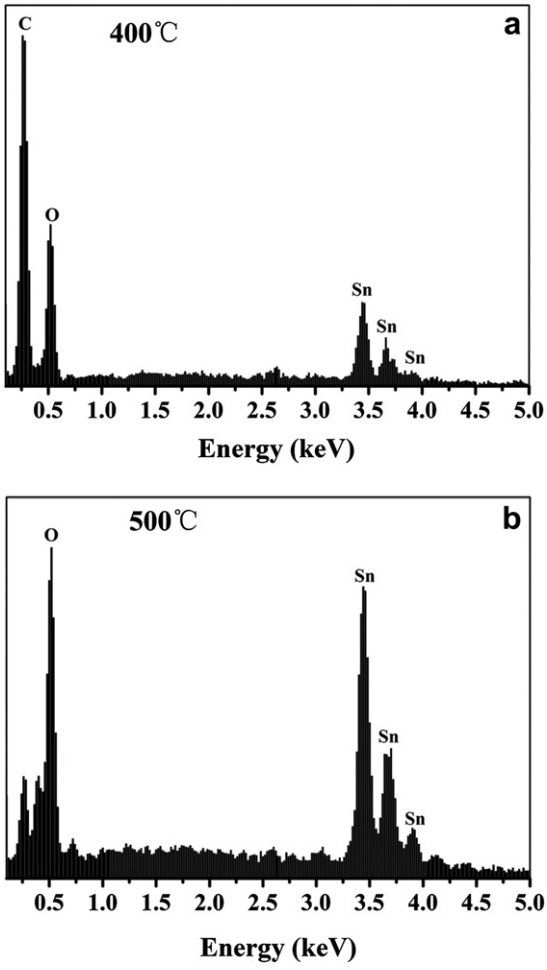

Fig. 2. EDS spectra of the obtained SnO_2@carbon nanofibers prepared at different calcinations temperatures: (a) 400 °C and (b) 500 °C.

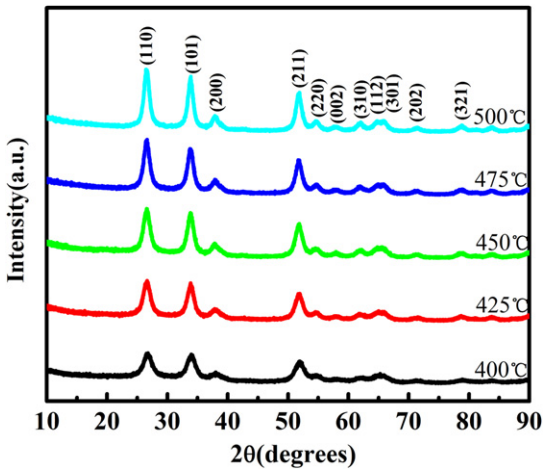

Fig. 3. X-ray diffraction patterns of as-prepared SnO_2@carbon nanofibers prepared at different calcinations temperatures.

obviously increases as the sintering temperature increases. The crystallite size of SnO_2 can be roughly estimated by the Debye–-Scherrer formula [16]:

$$d = 0.9\lambda/(\beta\cos\theta) \quad (1)$$

where d is average grain size, β the FWHM, λ the X-ray wavelength of Cu K_α radiation and θ the Bragg angle. The average crystallite sizes of these five samples calculated by the Scherrer equation using the data of (110) peaks are 4.3 nm (400 °C), 5.7 nm (425 °C), 6.2 nm (450 °C), 6.8 nm (475 °C), and 7.7 nm (500 °C), respectively.

The morphologies of SnO_2 NPs@carbon nanofibers sintered at different temperatures are shown in Fig. 4. Fig. 4a, c, e, g and i is the low-magnification SEM images of SnO_2 NPs@carbon nanofibers sintered at 400, 425, 450, 475, and 500 °C respectively, and the corresponding enlarged SEM images are shown in Fig. 4b, d, f, h, and j. The low-magnification SEM images reveal that each sample is composed of microfibers, and a large number of SnO_2 NPs can be clearly observed on carbon microfibers, which is shown in enlarged SEM images. The average size of SnO_2 NPs becomes larger as the sintering temperature increases, which is accorded with the result of XRD investigations. Moreover, the morphological characters of the original filter paper, a typical cellulosic structure, are faithfully inherited in the sintered samples. Indeed, the inset of Fig. 4a clearly reveals that the microfiber consists of many nanofibers coated with SnO_2 NPs. This structure is beneficial to improve the lithium-ion battery performance using SnO_2 NPs@carbon nanofibers as anode materials.

In order to further investigate the microstructure of the samples sintered at different temperatures, TEM has been used to analyze the samples. The typical morphologies of the SnO_2 NPs@carbon nanofibers are displayed in Fig. 5. Fig. 5a is the TEM image of the products sintered at 400 °C, which clearly shows the fibrous morphology with diameter about 200 nm. The nanofibers are amorphous carbon and a large number of SnO_2 NPs cover the surface of carbon nanofibers. The diameter of SnO_2 is about 4 nm as shown in inset of Fig. 5a. With increasing the sintering temperature, carbon nanofibers shrink obviously, meanwhile, the size of SnO_2 NPs increases. Fig. 5a–c clearly reveals this morphology evolution. When the sintering temperature increases to 475 °C, carbon nanofibers are oxidized (burnt off) because of the high sintering temperature, and then SnO_2 NPs are the majority of the sample as shown Fig. 5d. As the temperature further increases to 500 °C, the sample consists only SnO_2 NPs as shown in Fig. 5e, and the corresponding selected-area electron diffraction (SAED) pattern

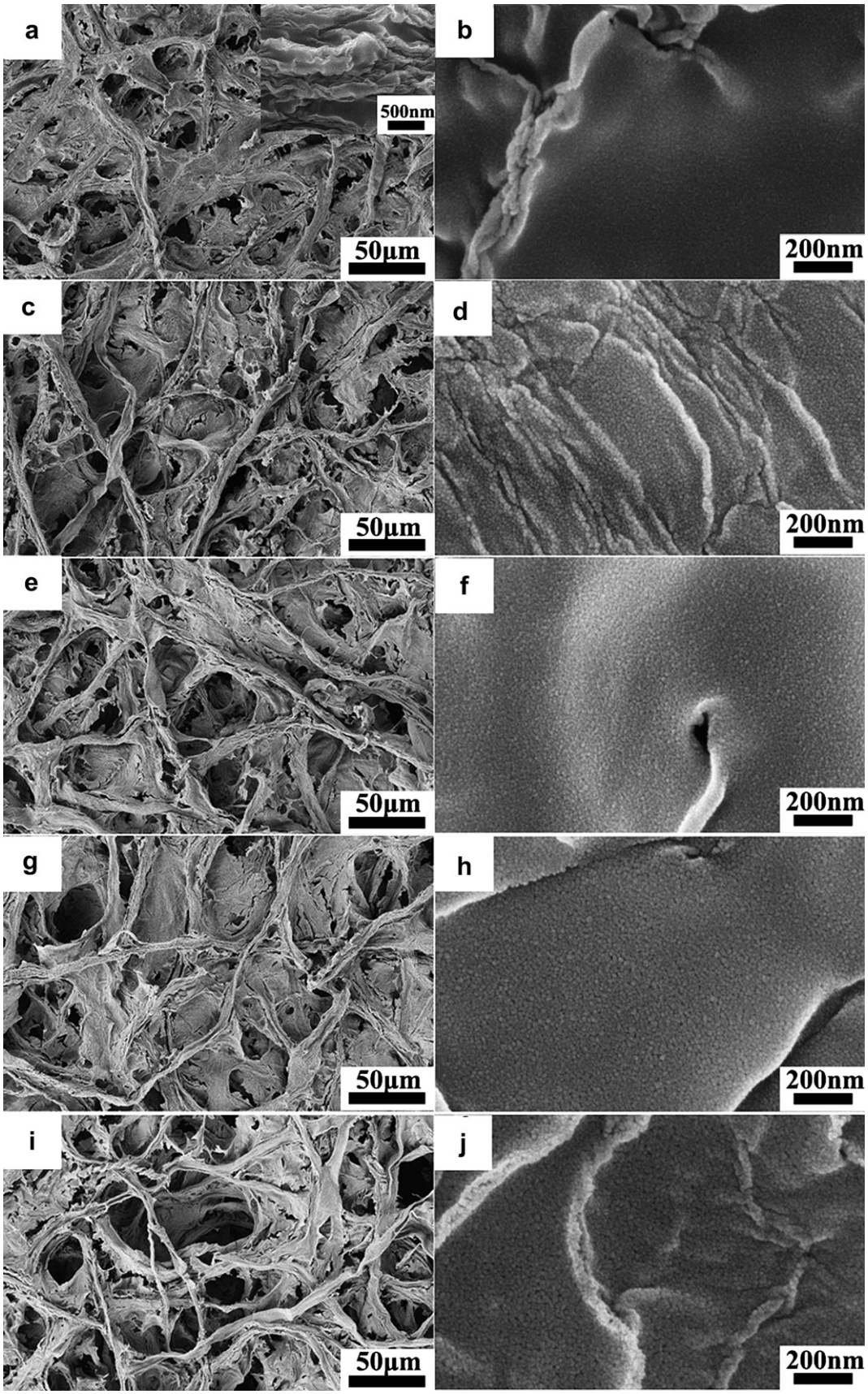

Fig. 4. SEM images of the obtained SnO_2@carbon nanofibers. The sintering temperatures are: (a,b) 400 °C, (c,d) 425 °C, (e,f) 450 °C, (g,h) 475 °C, (i,j) 500 °C.

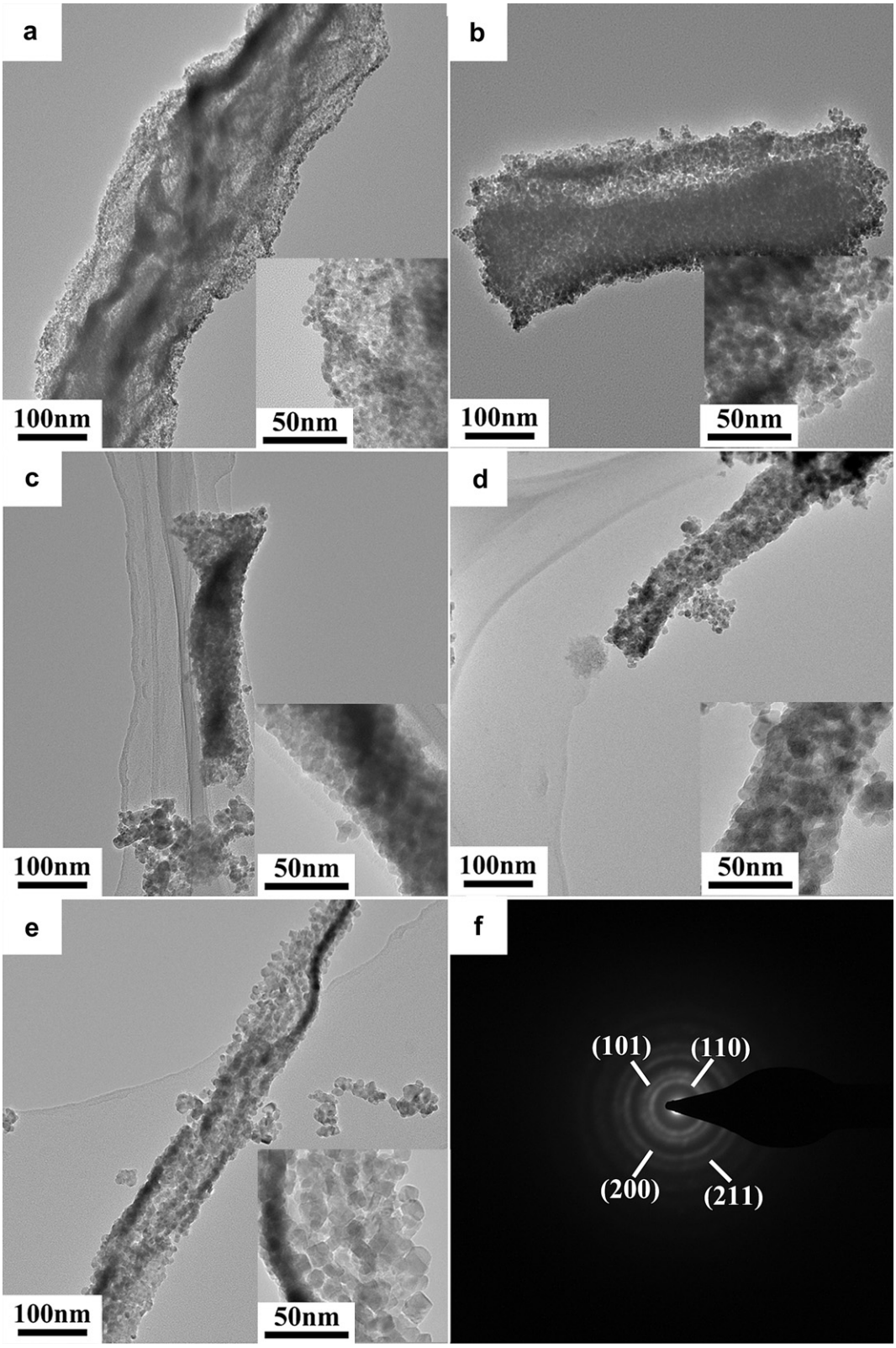

Fig. 5. TEM images of the obtained SnO_2@carbon nanofibers prepared at different calcinations temperatures: (a) 400 °C, (b) 425 °C, (c) 450 °C, (d) 475 °C, (e) 500 °C. (f) the corresponding SAED pattern of the sample shown in (b).

can be indexed as (110), (101), (200), (211) diffraction planes of tetragonal rutile-type SnO_2 as shown in Fig. 4e. In addition, the enlarged TEM images shown in the insets of Fig. 5 indicate that the size of SnO_2 NPs increases from 4 to 10 nm as the sintering temperature increases from 400 to 500 °C, which is consistent with the XRD investigations.

For quantifying the amount of carbon in the as-prepared SnO_2 NPs@carbon nanofibers, thermogravimetric analysis was carried

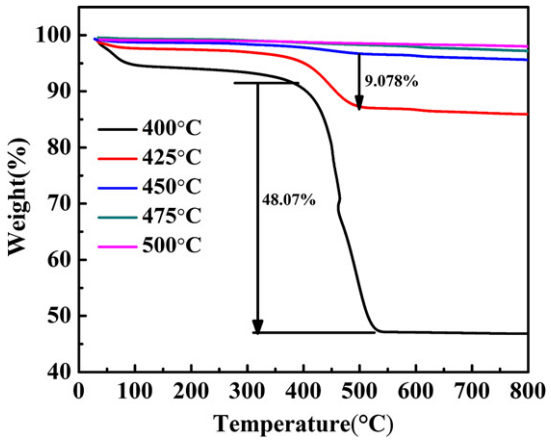

Fig. 6. Thermogravimetric analysis of SnO_2@carbon nanofibers prepared at different calcinations temperatures.

out in air atmosphere. The samples were heated from 25 to 800 °C at a rate of 10 °C min^{-1}. Fig. 6 shows the TGA of the SnO_2 NPs@carbon nanofibers prepared at different temperatures, displaying two weight loss regions. It clearly indicates that the two weight losses mainly take place at the temperature below 600 °C. The first weight loss occurs in the temperature range of 40–160 °C corresponding to the removal of water and the residual organic molecular absorbed on the samples, while the second weight loss in the temperature range of 200–500 °C is ascribed to the oxidation of the carbon nanofibers. The carbon is burn off at the temperature over 600 °C for all samples. Therefore, according to the change in weight before and after the oxidation of carbon, the weight of carbon in samples can be calculated, which is 48.1%, 9.1%, 1.5%, 0.9% and 0.8% for the samples prepared at 400, 425, 450, 475, and 500 °C, respectively.

The SnO_2 NPs@carbon nanofibers were employed as active materials to assemble laboratory lithium-ion battery. Fig. 7 shows the discharge capacity and Coulombic efficiency versus cycle numbers at a current density of 100 mA g^{-1}. The initial discharge capacities are 1315.2 mAh g^{-1} (400 °C), 1552.6 mAh g^{-1} (425 °C), 1568.9 mAh g^{-1} (450 °C), 1604.4 mAh g^{-1} (475 °C) and 1847.2 mAh g^{-1} (500 °C), which clearly indicate that the discharge capacity increases with decreasing the content of carbon in samples. However the discharge capacities of the samples prepared at high temperatures (less carbon in samples) decline quickly. After 30 cycles, the capacities are 362.2 mAh g^{-1} (400 °C), 383.1 mAh g^{-1} (425 °C), 275.2 mAh g^{-1} (450 °C), 271.2 mAh g^{-1} (475 °C) and 276.8 mAh g^{-1} (500 °C), which correspond to 27.5%, 24.7%, 17.5%,

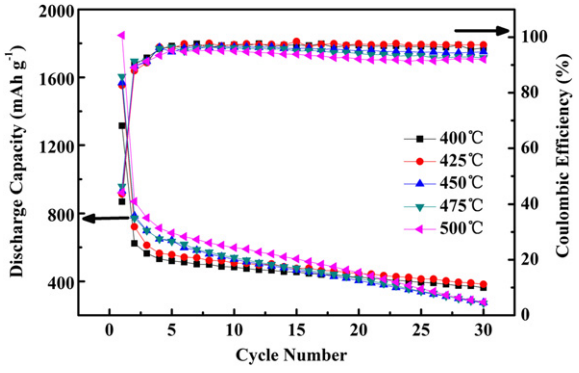

Fig. 7. The discharge capacity and Coulombic efficiency versus cycle numbers for SnO_2@carbon nanofibers prepared at different calcinations temperatures. The voltage window is set between 0.05 and 1.5 V, and the current density is 100 mA g^{-1}.

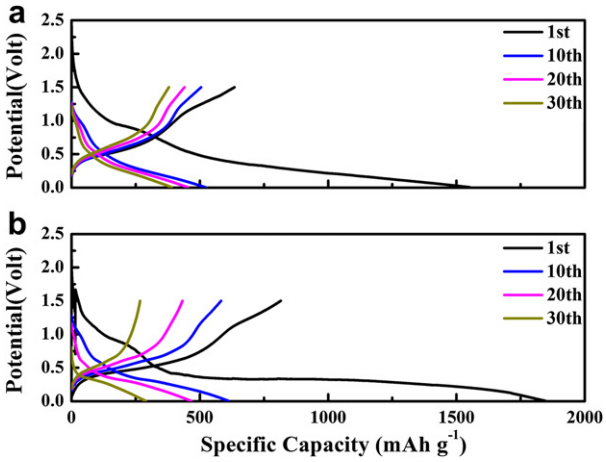

Fig. 8. Galvanostatic discharge/charge voltage profiles of the cells using SnO_2@carbon nanofibers prepared at different calcinations temperatures: (a) 425 °C and (b) 500 °C as anode active materials. Both cells were cycled between 5 mV and 1.5 V at a current density of 100 mA g^{-1}.

16.9%, 14.9% retention of their initial capacities, respectively. The initial Coulombic efficiencies are 40.9% (400 °C), 43.7% (425 °C), 44.8% (450 °C), 46.3% (475 °C) and 44.2% (500 °C), respectively. The formation of Li_2O and solid–electrolyte (SEI) interface during the first charge/discharge process are responsible for the low initial Coulombic efficiency. The Coulombic efficiency keeps steadily more than 90% after 5 cycles for all samples. For the samples containing more carbon (400 and 425 °C), the efficiency keeps steadily more than 97%, while for 500 °C sample, the efficiency is only about 90%. Fig. 8a and b shows the voltage profiles of the SnO_2@carbon nanofibers prepared at 425 °C and 500 °C at a current density of 100 mA g^{-1} within a voltage window of 0.005–1.5 V. The curves in Fig. 8 indicate that both anodes work in a narrow low-potential range (0–0.5 V) with flat and smooth voltage profiles. Although the cycling performance was not satisfactory, the capacity of the sample 425 (425 °C) faded much more slowly than that of the sample 500 (500 °C).

In order to explore the role of carbon nanofibers, the morphology of the cycled anode materials has been investigated. Fig. 9 shows an individual SnO_2@carbon nanofiber prepared at

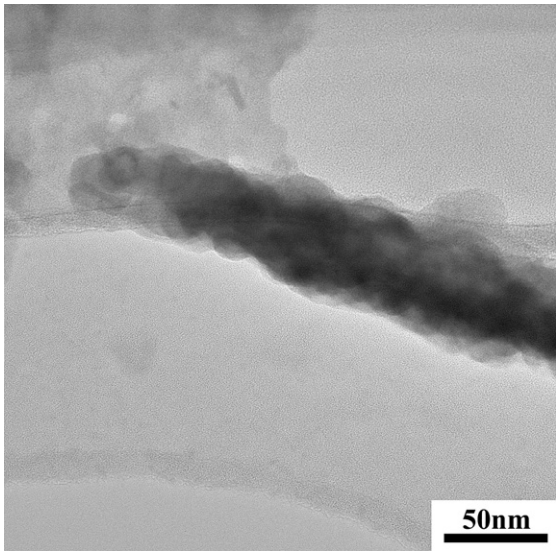

Fig. 9. TEM image of an individual SnO_2@carbon nanofiber prepared at 425 °C in the fully discharged state after 10 cycles.

425 °C after 10 charge–discharge cycles. After 10th charge/discharge, SnO_2 NPs aggregated into the larger particles with arbitrary shape and size due to their large volume change during lithiation/delithiation process, whereas the carbon nanofiber has been inherited. However Fig. 5 obviously shows that the carbon fibers already disappeared before the cycling when the sintering temperatures are increased to above 450 °C. Correspondingly, the performance of the sample (425 °C) is better than that of the samples sintering at the temperatures above 450 °C. Therefore we believe that the introduction of carbon nanofibers is clearly benefited to improve the cycle-life performance of SnO_2 anode. It is can be concluded that the carbon nanofibers effectively acted as a buffer layer during the electrochemical reaction to improve their performances.

4. Conclusions

In summary, a facile process was successfully introduced to synthesize large-scale SnO_2 nanoparticles (NPs)@carbon nanofibers as anode materials for lithium-ion battery. The weight of carbon in the samples was tuned by varying the sintering temperature. The carbon nanofibers were demonstrated to be beneficial to improve the cycling performance of lithium-ion battery. The method introduced in this study provided an easy strategy for the controlled introduction of carbon to optimize the performance of lithium-ion battery using SnO_2 NPs@carbon nanofibers as anode materials. Investigation shows that the sample with optimal content of carbon is sintered at 425 °C, with best specific capacity of 381 mAh g^{-1} after 30 cycles at a current density of 100 mA g^{-1}. In addition, the key features of this method are low cost, mass production and non-toxic source materials.

Acknowledgments

This work was supported by National Natural Science Foundation of China (No. 60976012), Program for New Century Excellent Talents in University, the Fundamental Research Funds for the Central Universities (No. 2011QNA3019), the Special-Program for the Science and Technology Plan of Zhejiang Province (2009C14005), and Science and Technology Innovative Research Team of Zhejiang Province (2009R50010).

References

[1] Y. Idota, T. Kubota, A. Matsufuji, Y. Maekawa, T. Miyasaka, Science 276 (1997) 1395–1397.
[2] J.P. Liu, Y.Y. Li, X.T. Huang, R.M. Ding, Y.Y. Hu, J. Jiang, L.J. Liao, J. Mater. Chem. 19 (2009) 1859–1864.
[3] I.A. Courtney, J.R. Dahn, J. Electrochem. Soc. 144 (1997) 2045–2052.
[4] D. Larcher, S. Beattie, M. Morcrette, K. Edstroem, J.C. Jumas, J.M. Tarascon, J. Mater. Chem. 17 (2007) 3759–3772.
[5] Y.L. Zhang, Y. Liu, M.L. Liu, Chem. Mater. 18 (2006) 4643–4646.
[6] P. Meduri, C. Pendyala, V. Kumar, G.U. Sumanasekera, M.K. Sunkara, Nano Lett. 9 (2009) 612–616.
[7] X.W. Lou, D. Deng, J.Y. Lee, L.A. Archer, J. Mater. Chem. 18 (2008) 4397–4401.
[8] C. Wang, Y. Zhou, J.Z. Jiang, J. Am. Chem. Soc. 132 (2010) 46–47.
[9] C.C. Chang, S.J. Liu, J.J. Wu, C.H. Yang, J. Phys. Chem. C 111 (2007) 16423–16427.
[10] S.M. Paek, E.J. Yoo, I. Honma, Nano Lett. 9 (2009) 72–75.
[11] S. Yang, H. Song, H. Yi, W. Liu, H. Zhang, X. Chen, Electrochim. Acta 55 (2009) 521–527.
[12] X.M. Sun, J.F. Liu, Y.D. Li, Chem. Mater. 18 (2006) 3486–3494.
[13] Z.H. Wen, Q. Wang, Q. Zhang, J.H. Li, Adv. Funct. Mater. 17 (2007) 2772–2778.
[14] G. Chen, Z.Y. Wang, D.G. Xia, Chem. Mater. 20 (2008) 6951–6956.
[15] J.S. Chen, Y.L. Cheah, Y.T. Chen, N. Jayaprakash, S. Madhavi, Y.H. Yang, X.W. Lou, J. Phys. Chem. C 113 (2009) 20504–20508.
[16] B.D. Cullity, Elements of X-ray Diffraction, Prentice Hall, Englewood Cliffs, NJ, 1978.